REPORT DOCUMENTATION PAGE

Form Approved OMB NO. 0704-0188

1. REPORT DATE (DD-MM-YYYY)	2. REPORT TYPE	3. DATES COVERED (From - To)
	Technical Report	-

4. TITLE AND SUBTITLE
Progress report for 10-1-2014 to 10-1-2015

5a. CONTRACT NUMBER
W911NF-13-1-0107

5b. GRANT NUMBER

5c. PROGRAM ELEMENT NUMBER

6. AUTHORS
Stuart S.P. Parkin, See-Hun Yang

5d. PROJECT NUMBER

5e. TASK NUMBER

5f. WORK UNIT NUMBER

7. PERFORMING ORGANIZATION NAMES AND ADDRESSES
IBM Corporation (Almaden Research Cente
650 Harry Road

San Jose, CA 95120 -6099

8. PERFORMING ORGANIZATION REPORT NUMBER

9. SPONSORING/MONITORING AGENCY NAME(S) AND ADDRESS (ES)
U.S. Army Research Office
P.O. Box 12211
Research Triangle Park, NC 27709-2211

10. SPONSOR/MONITOR'S ACRONYM(S)
ARO

11. SPONSOR/MONITOR'S REPORT NUMBER(S)
63248-CS-ACI.1

12. DISTRIBUTION AVAILIBILITY STATEMENT
Approved for public release; distribution is unlimited.

13. SUPPLEMENTARY NOTES
The views, opinions and/or findings contained in this report are those of the author(s) and should not contrued as an official Department of the Army position, policy or decision, unless so designated by other documentation.

14. ABSTRACT
This report details progress for the period 10-1-2014 to 10-1-2015

15. SUBJECT TERMS
Racetrack Memory, Spintronics

16. SECURITY CLASSIFICATION OF:			17. LIMITATION OF ABSTRACT	15. NUMBER OF PAGES	19a. NAME OF RESPONSIBLE PERSON
a. REPORT	b. ABSTRACT	c. THIS PAGE			Stuart Parkin
UU	UU	UU	UU		19b. TELEPHONE NUMBER 408-927-2390

Report Title

Progress report for 10-1-2014 to 10-1-2015

ABSTRACT

This report details progress for the period 10-1-2014 to 10-1-2015

W91NF1310107 Progress Report for 10/01/2014 ~ 10/01/2015

Highlights

- **Paper published in Nature Nanotechnology describing our discoveries of (i) record-breaking current driven domain wall velocities in racetracks formed from synthetic antiferromagnets and (ii) a novel giant exchange torque**
- **Invited Commentary published in Nature Nanotechnology describing the evolution of Racetrack Memory over 4 distinct generations**
- **Discovery of the current driven precession of domain walls in synthetic antiferromagnetic racetracks**
- **Discovery of novel racetrack in which the threshold current for the motion of domain walls is reduced by 4 orders of magnitude**

I. Anomalous Walker breakdown in synthetic antiferromagnet (SAF) racetracks

1. Introduction and Motivation

Previously, we reported a novel mechanism to move domain walls (DWs) with nanosecond long current pulses in single racetrack nanowires formed from perpendicularly magnetized ultra-thin films interfacing non-magnetic heavy metal layers: the Chiral Spin Torque, the combined mechanism of spin Hall effect and Dzyaloshinsky-Moriya interaction (DMI) [1]. The CST is distinct from conventional spin transfer torque (STT) allowing for much more efficient manipulation of DW motions in nanowires for Racetrack Memory [2]. However, the DWs in perpendicularly magnetized racetracks are subject to significant demagnetizing fields that give rise to interactions between the DWs limiting device density. Recently, to overcome this obstacle we have constructed racetracks that have no net magnetization by forming them from synthetic antiferromagnets (SAF) [3]. We show that not only domain walls can be moved with current in such racetracks with nano-second long current pulses but the domain walls move even faster than in nanowires which have a non-zero magnetization. The SAF nano-wires are formed from synthetic antiferrromagnets, namely sandwiches of perpendicularly magnetized nano-wires coupled antiferromagnetically via ultrathin ruthenium layers. The domain walls in one layer are mirrored exactly in the other layer. We have discovered that the large antiferromagnetic exchange-coupling that arises from the Ru layer, gives rise to a novel giant exchange coupling torque (ECT) that drives the domain walls much

more efficiently and at speeds several times higher than in nearly identical ferromagnetically coupled sandwiches (SF). We have found record-breaking domain wall velocities of almost 1,000 m/s. We have shown that the ECT is allowed only in SAF structures but not in SF nanowires. Our breakthrough discovery was published in Nature Nanotechnology [3] last month together with an invited commentary in which we reviewed our advances in Racetrack Memory over the past 10 years [2]. We have also developed a detailed analytical model that can account for our remarkable experimental findings and gives insight into the physics behind the current induced domain wall motion in SAF and SF racetracks.

The SAF structure is composed of two magnetic sublayers that are exchange-coupled antiferromagnetically via an ultra thin Ru spacer layer. This complex structure more than doubles the number of parameters that govern the DW dynamics compared to a single layer or SF racetrack, thereby giving rise to richer physics, and a wealth of new phenomena that can be manipulated by only slight changes in the racetrack structure. For example, our newly developed model to account for the DW dynamics in SF and SAF nanowires predicts that the DW magnetizations precess /oscillate and the DWs move back and forth by application of current pulses when, (1) the AF exchange coupling within the SAF structure is not too strong, (2) the net magnetization of the SAF structure is small, i.e, the moments of the two sub-racetrack layers that comprise the SAF are nearly compensated, and (3) a longitudinal field is applied parallel to the racetrack so that one sublayer is exerted to a much larger longitudinal field torque than the other. This interesting phenomenon of current driven DW precession and oscillation is reminiscent of field or current driven Walker Breakdown (WB) that results from a demagnetizing field torque [4] or a non-adiabatic spin transfer torque [5], respectively, in conventional in-plane soft magnetic systems. During this period of the ARO program, we found that distinct from conventional WB, the DWs in SAF nanowires are forced to precess by a large disparity in the DW driving torque in the two sublayers (which is, of course, not possible in SF or single layer nanowires). Below we present these exciting new results and discuss how the WB takes place in SAF racetracks. Since the position of the DW in one sublayer is locked to that in the other sublayer, the total DW velocity in the SAF structure is determined by the weighted average of the current induced torques on the individual sublayer DWs. When, for instance, the driving torque on the lower sublayer is significantly larger than that in the upper sublayer, the difference between the torques inflicted on the individual sublayer DWs can be very large. This big discrepancy in torque can destabilize and result in the precession of the SAF DW.

Since the ECT in the SAF structure drives both sublayer DWs in the same direction cooperatively, a not very large ECT is needed to observe this anomalous WB. One of the most accessible ways to observe this precession is by the application of a longitudinal field, which increases the torque discrepancy as we will see in the next subsection.

2. Experimental Results and conclusions

The SAF structures used to study the anomalous WB are shown in Fig. 1 (upper left). All films were grown on Si(100) | 250 Å SiO_2 substrates at room temperature by magnetron

sputtering at an Ar pressure of 3 mTorr. The devices were patterned with standard photo-lithography followed by Ar ion etching. The measured devices here were 50 μm long and 2 μm wide. The values of M_R/M_S decrease with Co layer thickness, where M_R and M_S are the remnant and saturation magnetizations, respectively (see Fig. 1 upper right) thus showing that for all samples $M_L > M_U$ where M_L (M_U) is lower (upper) sublayer magnetic moment per unit area. Although the nominal thickness of the lower sublayer is smaller than that of the upper sublayer, the proximity induced magnetization (PIM) at the lower Pt/Co interface increases the M_L magnitude substantially [6]. This PIM in Pt layer induces a much larger DMI in the lower sublayer compared to the upper sublayer, which consequently gives rise to a large difference in DMI field torques on M_L and M_U when current pulses are applied.

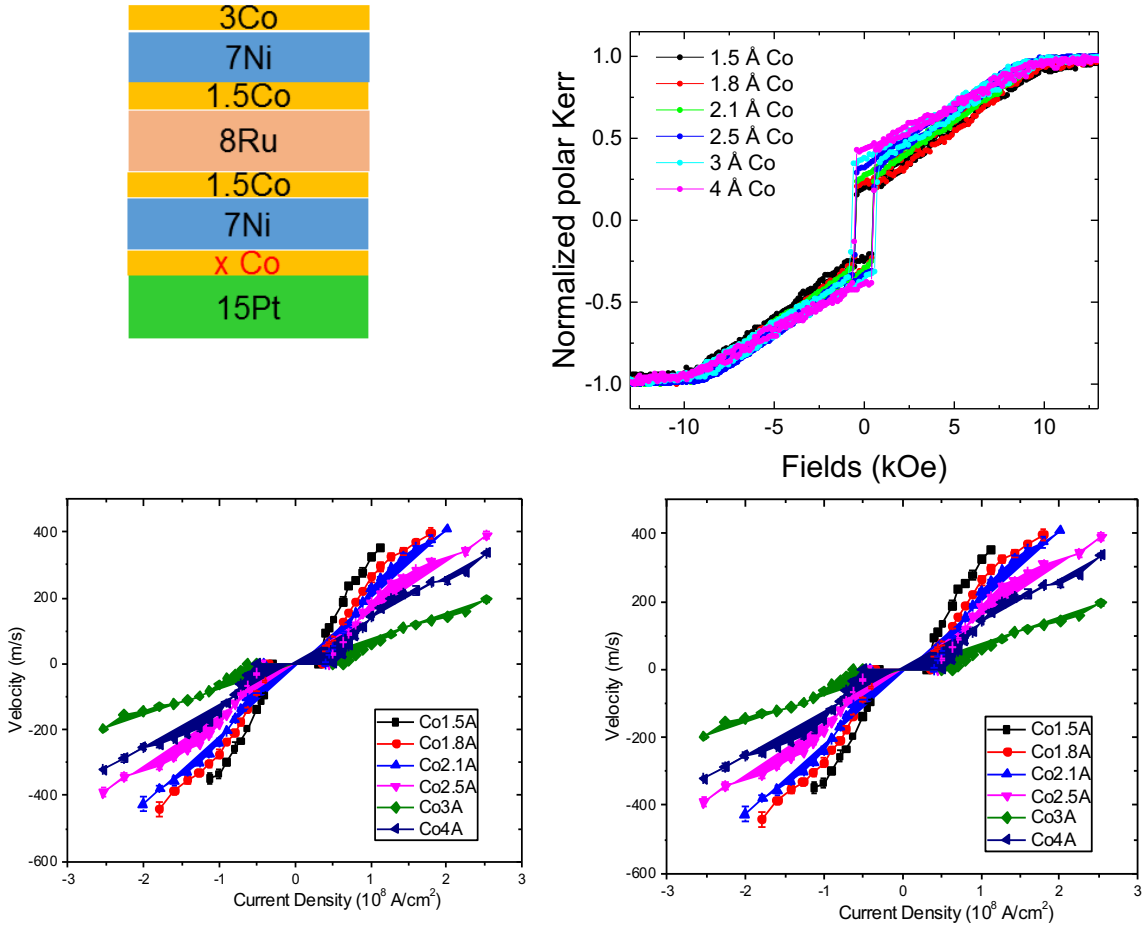

Fig. 1. (top left) The SAF structure for anomalous WB study where the bottom-most Co layer thickness is varied. 20 Å TaN is placed underneath 15 Å Pt layer, and 50 Å TaN layer is capped to protect the magnetic layer. Here all thicknesses are in Ångstroms. (top right) Normalized polar Kerr loop as a function of easy axis fields for various Co layer thickness. (bottom left) Up-down DW velocity vs current density as a function of Co thickness for various Co layer thickness. (bottom right) Up-down DW velocity vs longitudinal magnetic field H_x for various current density in nanowire formed from 15 Pt | 3 Co | 7 Ni | 1.5 Co | 8 Ru | 1.5 Co | 7 Ni | 3 Co. Here 5 ns long current pulses were used.

As current is flowed along the wire (longitudinal direction), spin current is generated via the spin Hall effect (SHE) within the Pt layer along an out-of-plane direction with a spin polarization that is directed transverse to the wire. The spin current can also arise in the Ru

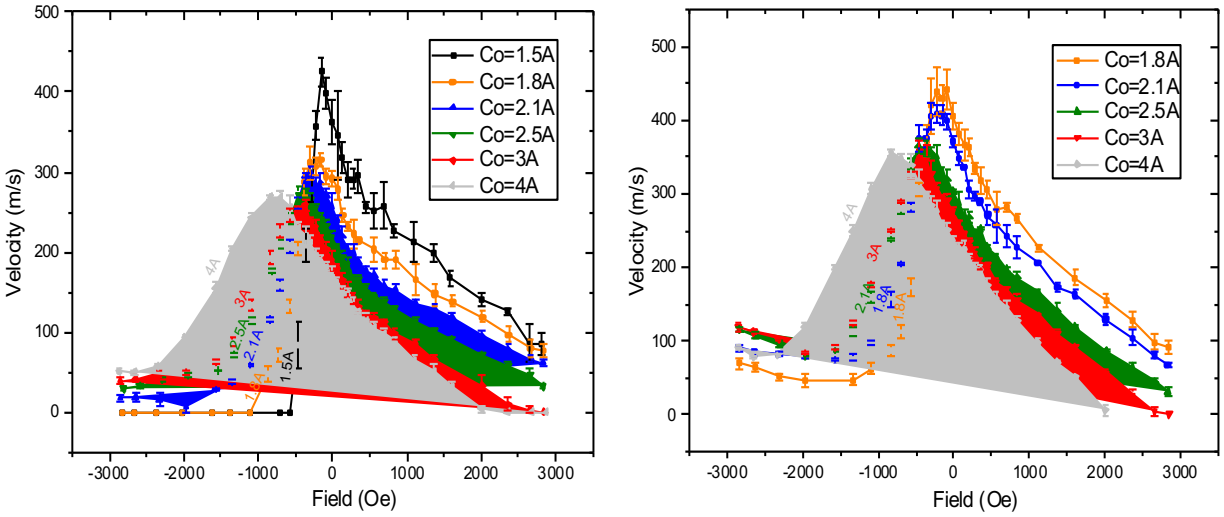

Fig. 2. Up-down DW velocity vs longitudinal magnetic field H_x for various Co thicknesses. Current density 1.05×10^8 A/cm^2 (left) and $1.67 \times 05 \times 10^8$ A/cm^2 (right) are applied, respectively. $H_x < 0$ region correspond to the Walker breakdown where the DW velocity drops abruptly as $| H_x |$ increases. Here 5 ns long current pulses were used. The error bars correspond to one standard deviation.

AF coupling layer [7] but the Ru spin diffusion length (> ~ 2nm) [8] is much larger than the Ru layer thickness (8 Å) at room temperature, which nearly cancels out the spin accumulation at the Co/Ru and Ru/Co interfaces thus ending up with very little spin Hall torque from the Ru layer. Consequently, the spin Hall torque on M_L would be much larger than that on M_U. Although the spin Hall torque does not directly displace the DWs, it is the main driving force that rotates the DW magnetization in an azimuthal direction since the spin Hall torque is dominantly damping-like in Pt/Co based nanowires. Hence, the total azimuthal motion torque on M_L would be the summation of the spin Hall torque (counter-clockwise) and the M_U-dragging induced torque (clock-wise). On the other hand, the torque on M_U is governed dominantly by the M_L-driving induced torque (anti-clockwise). Here damping torques induced from DW displacement are usually very small [3]. As a result, the M_U keeps on processing clockwise due to the M_L driven torque. On the other hand, in M_L two torques, i.e, spin Hall torque and M_U-dragging torque compete with each other, as mentioned above. When the M_U-dragging torque happens to be larger (smaller) than the spin Hall torque, M_U rotates in clockwise (anti-clockwise) depending on where M_U is located, which leads to a precessional oscillation of M_L in the azimuthal direction (see Fig. 3).

Finally, this dynamically induced WB destabilizs the DW dynamics so that the DW moves back and forth, thereby dramatically reducing the average DW velocity. As M_L (or M_R) increases against M_U (or M_S), the WB region systematically shifts to negative H_x (see Fig. 2). An increase of M_L gives rise to changes in many parameters; increase of H_{DML}, decrease of H_{SHU}, increase of anisotropy, and decrease of domain wall width Δ. Our model, that takes all of these changes into account, agrees well with the velocity vs. H_x for various M_L, M_U and current density J.

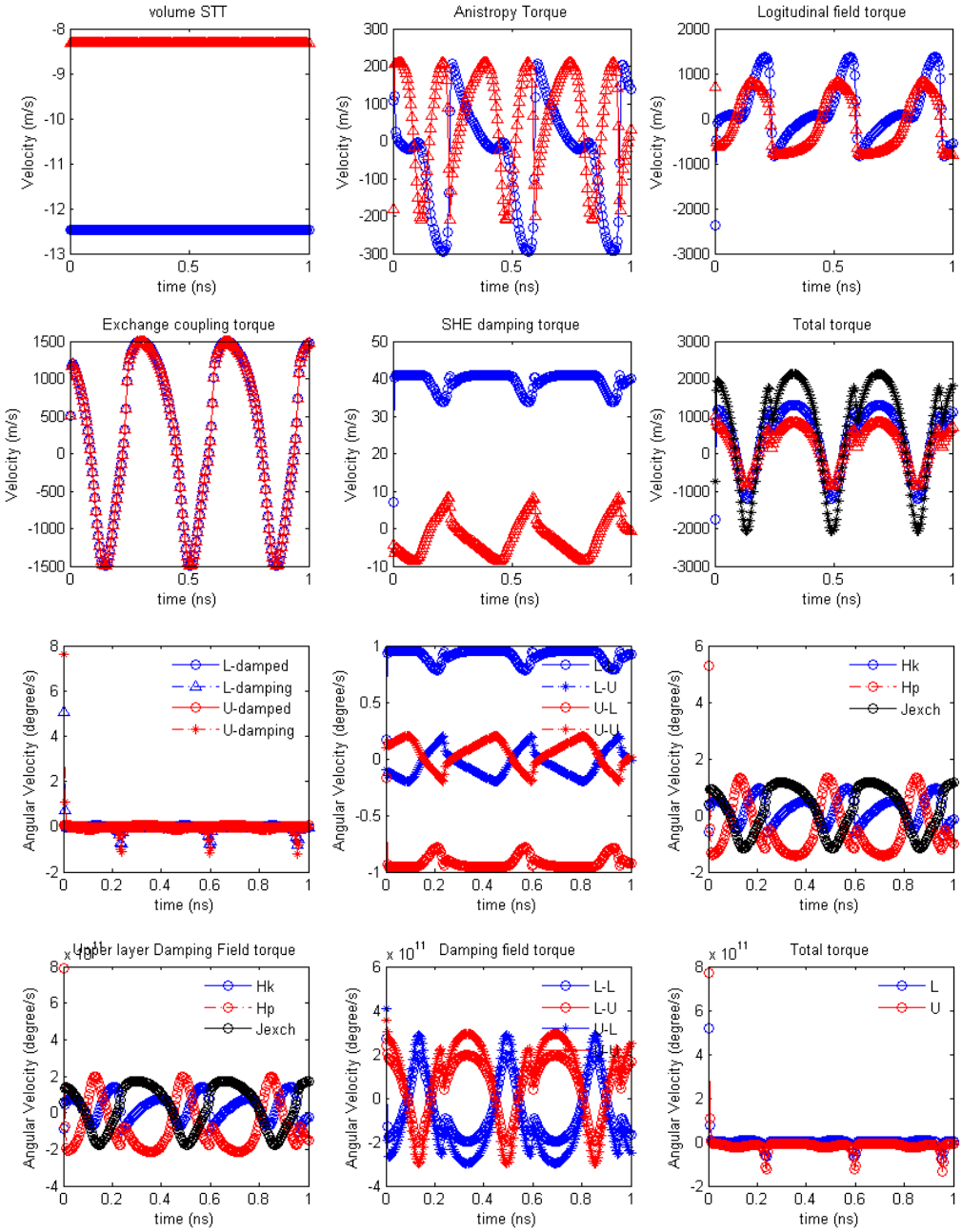

Fig. 3. Upper six panels: Calculated DW velocities and decomposed velocities driven by various torque components in WB region. Lower six panels: Calculated azimuthal angular velocities and decomposed velocities driven by various azimuthal torque components in WB region. Here the used parameters are M_L=600 emu/cc, M_U=400 emu/cc, J=-0.1 erg/cm^2, H_{SHL}=580 Oe, H_{SHU}=180 Oe, H_{DML}=-1400 Oe, H_{DMU}=300 Oe, H_{kL}=1400 Oe, H_{kU}=1400 Oe, H_x=-2000 Oe, Δ=4.3 nm, u_L=21 m/sec, u_U=21 m/sec, α_L=0.1, α_U=0.1, βL=0 and β_U=0.

3. Future plans

The WB in SAF PMA wires is not only very interesting but is of potential use for the development of nano-oscillators. We are exploring and tuning the structure parameters to optimize this WB behavior.

II. Low critical current and potentially high spin Hall angle from racetrack nanowires with Pt-Bi and Pd-Bi alloy insertion layers

1. Introduction and Motivation

Although our recent breakthrough in highly efficient ECT driven DW motion from SAF PMA racetracks with no net magnetization overcomes all scientific obstacles to the development of high-density and high-performance storage class memory devices, there remains several technical barriers to implement this in integrated chips. One of them is the high critical threshold current density J_c above which the DWs start to move. Typical J_c values are ~ $5x10^7$ A/cm^2 and 2-$3x10^7$ A/ cm^2 for single layer and SAF racetracks, respectively, which are larger than what can be accommodated for transistor switches in Racetrack Memory. To resolve this challenge, during this period of our program, we have explored new materials and schemes that can lower J_c values significantly. In particular, we have focused on Bi alloys since Bi is a heavy semi-metal with very high spin-orbit interaction (SOI). Thus, we could anticipate a very high charge to spin current ratio, i.e, spin Hall angle (SHA), thus giving rise to higher spin Hall torques than from Pt and Pd, and thereby potentially lowering J_c in racetrack nanowires when alloyed with Pt and Pd. Here we show that J_c is lowered significantly from ~$5x10^8$ A/ cm^2 to ~$2x10^8$ A/cm^2 when 8 Å Pt-Bi thin layers are inserted between the Pt underlayer layer and the first Co layer, which may be likely due to enhanced spin Hall angle generated by Pt/Pt-Bi layers.

In other results, using novel resistive underlayers, we have observed a reduction in Jc by more than 4 orders of magnitude. These results which are extremely interesting and exciting for future racetrack memory technologies will be reported in the next quarterly report.

2. Results, Discussion and Conclusion

Films were grown and patterned in the same way as described above. 0, 1, 2, 4, 6, and 8 Å thick $Pt_{75}Bi_{25}$ and $Pd_{50}Bi_{50}$ layers were inserted between 15 Å Pt and 3 Å Co layers (see Fig. 5a,b insets). First, magnetic properties were measured by polar Kerr and SQUID to check the PMA quality, anisotropy constants K and K_{eff}, and magnetizations M_s that are critical to understand the DW dynamics. These measured data are summarized in Table 1. K, K_{eff} and M_s values decrease with increasing Pt-Bi and Pd-Bi layer thicknesses, and are more steeply reduced for Pd-Bi, which supports our model [6] that a substantial magnetization is induced in Pt layer by proximity effect with interfacing Co layer and closely involved with anisotropy and DMI strengths D as we discuss later.

Base frame	***15ÅPt/XÅPt/Bi(75/25)*/3ÅCo/7ÅNi/1.5ÅCo***									
Underlayer	***Reference***	***Pt/Bi (75/25)***					***Pd/Bi (50/50)***			
Sample #	*1*	*3*	*5*	*7*	*8*	*9*	*11*	*13*	*14*	*15*
X (Å)	*0*	*1*	*2*	*4*	*6*	*8*	*1*	*2*	*4*	*6*
M_s *(emu.cm^{-3})*	*600*	*570*	*490*	*480*	*510*	*470*	*510*	*500*	*500*	*450*
K (10^{6}erg.cm^{-3})	*5.1*	*5.1*	*4.3*	*4*	*3.8*	*3*	*4.7*	*4*	*3.7*	*2.6*
K_{eff} *(10^{6}erg.cm^{-3})*	*2.9*	*3.1*	*2.8*	*2.6*	*2.2*	*1.6*	*3*	*2.5*	*2.1*	*1.3*
H_k *(kOe)*	*1.5*	*1.5*	*1.2*	*1.2*	*1.2*	*0.9*	*1.3*	*1.2*	*1.1*	*0.8*

*or Pd/Bi(50/50).

Table 1. Magnetic properties measured by SQUID on 20 TaN | 15 Pt | x Pt-Bi or Pd-Bi | 3 Co | 7 Ni | 1.5 Co | 15 TaN. All numbers are in Ångstroms.

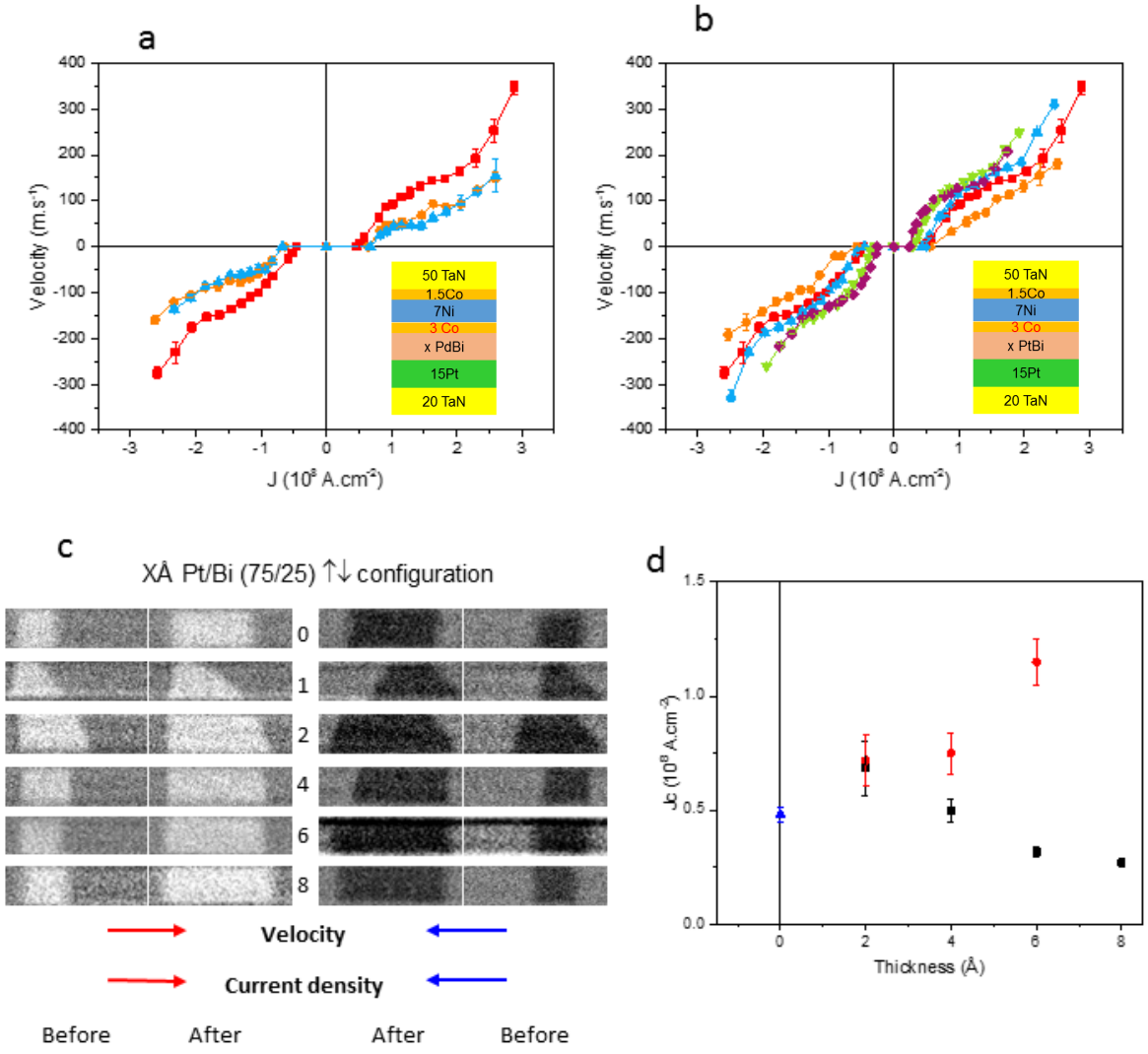

Figure 4: Current induced DW motion in Pt-Bi and Pd-Bi layer inserted PMA nanowires. DW velocity vs. current density for various Pt-Bi and Pd-Bi thickness with 5ns long current pulses for **a**, Pd/Bi(50/50) and **b**, Pt/Bi(75/25) where 0Å (red squares), 2Å (orange circles) and 4Å (blue up-triangles), 6Å (green down-triangles) and 8Å (purple diamonds). The error bars correspond to one standard deviation. **c**, Kerr microscope images of up-down single DW moving along a nanwire with Pt-Bi insertion layer. Brighter (darker) area correspond to up (down) domains. Left (right) two columns correspond to the case that the current flows from the left (right) to the right (left). In the left (right) two columns, the left (right) column represents the domain images before application of current pulses while the right (left) column displays the image after the current pulses is applied showing that DW moves along current flow direction. **d**, Pd-Bi and Pt-Bi thickness dependence of threshold current density: control sample with no Pd-Bi or Pt-Bi (blue up-triangle), Pd/Bi (red circle) and Pt/Bi (black square). The errors bar correspond to the max and min value accessible with the pulse generator.

Current driven DW motions show significantly different trends for Pd-Bi and Pt-Bi layer insertions as a function of their respective thicknesses. First, for Pd-Bi the DW velocity decreases while J_c increases monotonically, with increasing Pd-Bi thickness at a given

current density. On the other hand, the DW motion becomes slower for a 1-2 Å Pt-Bi interface layer where J_c forms a maximum, but for thicker Pt-Bi layers, the DWs move faster and J_c decreases (see Fig. 4a,b,d). This non-monotonic behavior in Pt-Bi may be correlated with DW tilting as shown in Fig. 4c.

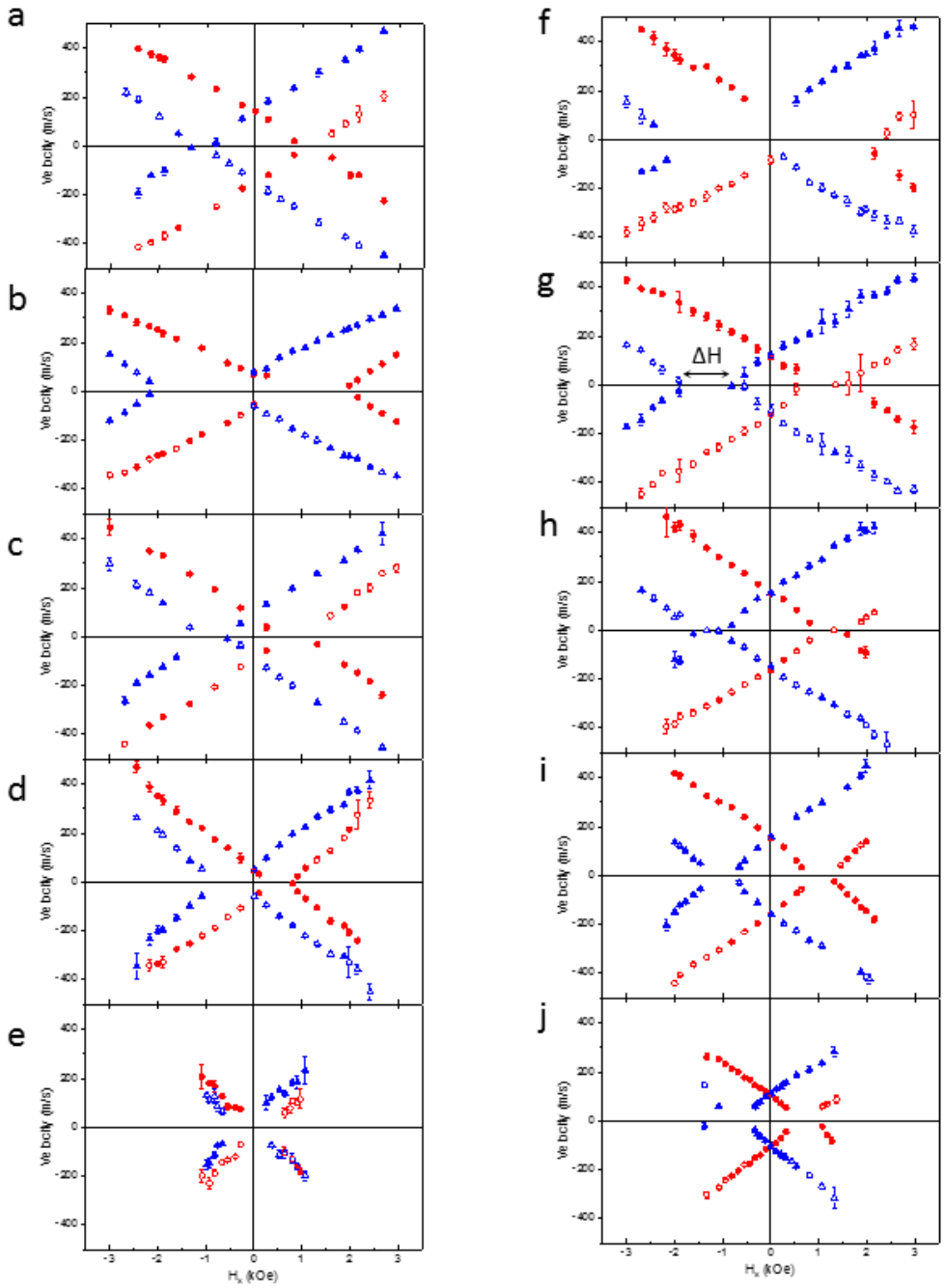

Figure 5: DW velocity vs longitudinal magnetic field H_x for various Pd-Bi and Pt-Bi thicknesses. a-j Filled (empty) symbols correspond to positive (negative) current pulses application. Red (blue) symbols correspond to the up-down (down-up) DW configurations. **a**, 0Å Pt-Bi or Pd-Bi; **b** 1Å Pd-Bi, **c**, 2Å Pd-Bi, **d**, 4Å Pd-Bi, **e** 6Å Pd-Bi **f,** 1Å Pt-Bi, **g**, 2Å Pt-Bi, **h**, 4Å Pt-Bi **i**, 6Å Pt-Bi, **j** and 8Å Pt-Bi. The error bars correspond to one standard devivation. 5 ns long current pulses are used, and current density are **a**, 2.0, **b**, 1.5, **c**, 1.8, **d**, 1.6, **e**, 0.85, **f**, 1.9, **g**, 2.2, **h**, 1.7, **i**, 1.4, and **j**, 0.8 in 10^8A/cm^2.

DWs are tilted by the interplay of a chiral Neel wall induced by DMI and SHE during the application of current pulses [9,10]. The DW tilting disappears when the DW energy is large enough to minimize the DW length and the pinning of DW is small. A large tilting angle found in the nanowire with 1 -2 Å Pt-Bi layer implies that the pinning is significant likely due

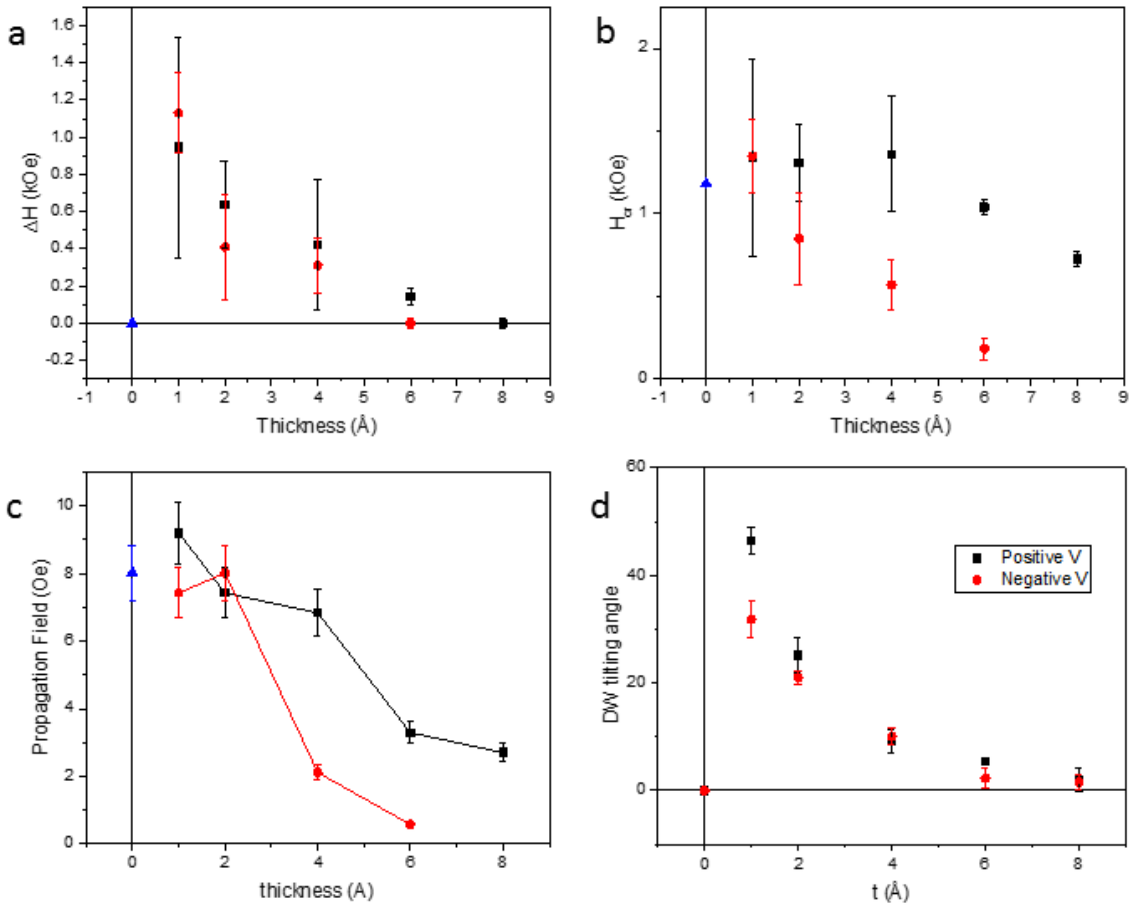

Figure 6 | Key parameters measured from current driven motion as a function of Pt-Bi and Pd-Bi thickness a, Measured flat field range ΔH, **b**, crossing field H_{cr} obtained from Fig. 6, **c**, measured propagation fields **d**, DW tilted angles for up-down domain configuration. Each symbol correspond to no Pt-Bi or Pd-Bi (blue up-triangle), Pd/Bi (red circle) and Pt/Bi (black square). The error bars correspond to one standard deviation.

to incomplete coverage of Pt-Bi layer on Pt thus causing inhomogeneous anisotropy, DMI and spin Hall causing lots of pinning sites in the wire. As the Pt-Bi layer becomes thicker fully covering the Pt layer, not only do the pinning sites decrease recovering J_c but J_c becomes even smaller than the nanowires with no Pt-Bi layer. The J_c values appear to be correlated with the propagation field H_p for wires with Pt-Bi layer to some extent but in contrast look to be anti-correlated with H_p for those with Pd-Bi layer (see Fig. 4d and Fig. 6c). Since it is known that the H_p is determined by the anisotropy K and K_{eff} (see Table 2), it seems that J_c has little to do with H_p (see Fig. 7e).

To understand the DW dynamics from the nanowires with Pt-Bi and Pd-Bi insertion layers, DW velocity was measured as a function of longitudinal field H_x (Fig. 5). H_{cr}, the field at

which DW does not move, monotonically decreases with increasing Pt-Bi and Pd-Bi thicknesses, which means that the DMI fields and DMI strengths decrease with these thicknesses (see Fig. 7c and Table 2). It is found that DMI fields and DMI constant D are closely correlated with the proximity induced magnetization in Pt-Bi and Pd-Bi and anisotropy, which in turn supports our previous model [6].

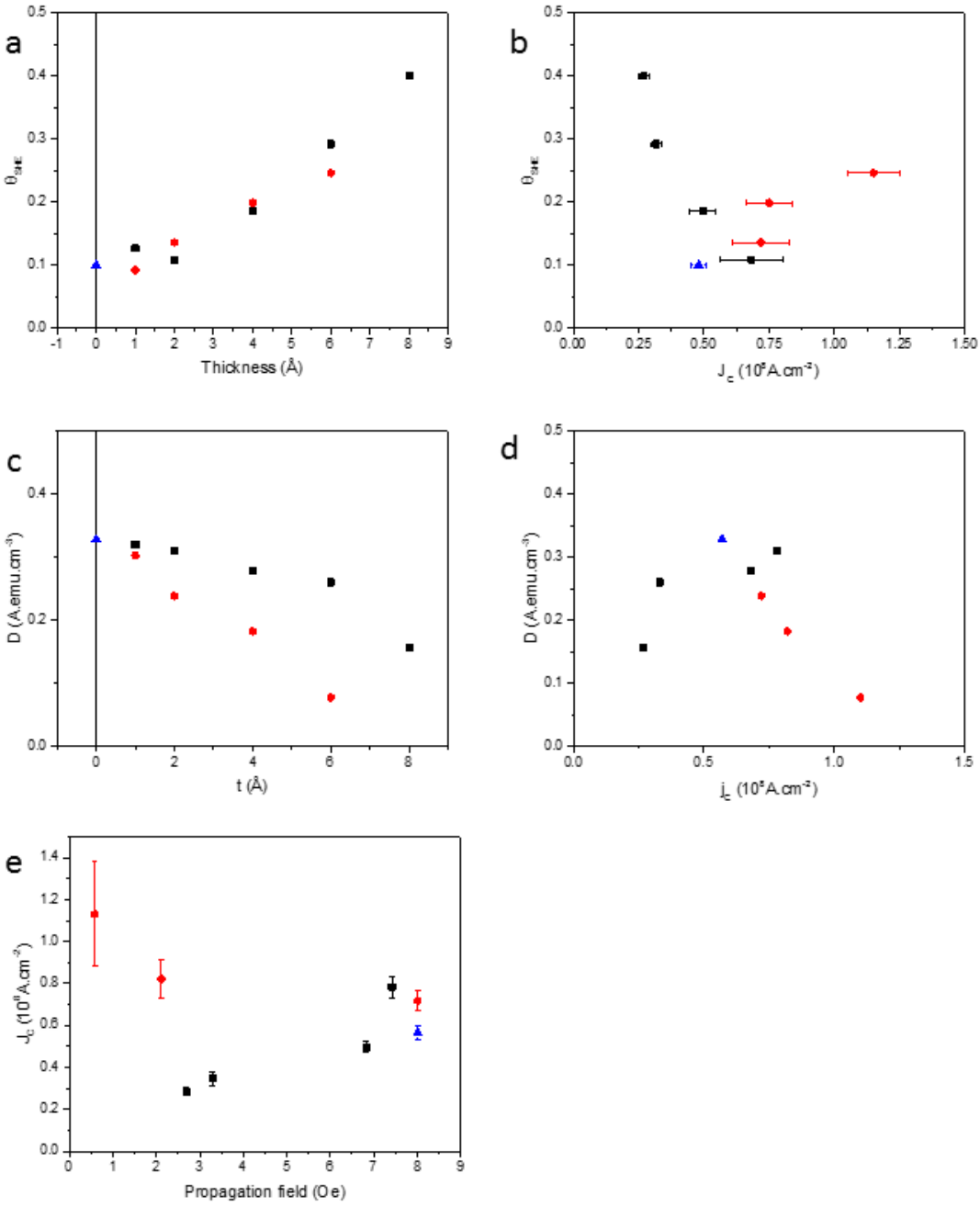

Figure 7: Pt-Bi and Pd-Bi thickness and J_c dependence of SHE and DMI. Spin Hall angles extracted from 1D model simulation as a function of **a**, the Pt-Bi and Pd-Bi layer thickness and **b**, J_c. DMI constant D obtained from 1D model simulation as a function of **c**, the Pt-Bi and Pd-Bi layer thickness and **d**, j_c (**e**) j_C vs propagation field. Each symbol correspond to no Pt-Bi or Pd-Bi (blue up-triangle), Pd/Bi (red circle) and Pt/Bi (black square). The error bars correspond to one standard deviation.

Although the error bars are substantial, we fitted the spin Hall angle from the velocity vs H_x curves within our 1D analytical model and found that the spin Hall angle for Pt-Bi layer may be as much as 0.4 for 8Å Pt-Bi. J_c seems to be correlated with the spin Hall angle. However, it is still premature to make a conclusion of what mostly determines the J_c from the data that we have collected to date (Fig. 7).

Table 2: Summary of measured magnetic properties and parameters obtained from 1D model fitting.

	Underlayer	Ref	PtBi (75/25)					PdBi (50/50)			
	Thickness (Å)	0	1	2	4	6	8	1	2	4	6
Measured Properties	M_s (emu.cm^{-3})	600	570	490	480	510	470	510	500	500	450
	δM_s (emu.cm^{-3})	0	30	110	120	90	130	90	100	100	150
	$\delta M_s/M_s$(ref) (%)	0	5	22	25	18	28	18	20	20	33
	K (10^6erg.cm^{-3})	5.1	5.1	4.3	4	3.8	3	4.7	4	3.7	2.6
	K_{eff} (10^6erg.cm^{-3})	2.9	3.1	2.8	2.6	2.2	1.6	3	2.5	2.1	1.3
	H_k(kOe)	1.5	1.5	1.2	1.2	1.2	0.9	1.3	1.2	1.1	0.8
Measured Properties	J (10^6A.cm^{-2})	2.0	1.9	2.2	1.7	1.4	0.8	1.5	1.8	1.6	0.9
	J_c (10^6A.cm^{-2})	0.57	-	0.78	0.68	0.33	0.27	-	0.72	0.82	1.10
	t_{pulse} (ns)	5.0	5.0	5.0	5.0	5.0	5.0	5.0	5.0	5.0	5.0
	H_{prop} (Oe)	8	9.2	7.4	6.8	3.3	2.7	7.4	9	2.1	0.58
	H_{DL} (kOe)	1.2	1.3	1.3	1.2	1	0.7	1.4	0.9	0.6	0.2
	ΔH (Oe)	0	0.95	0.64	0.42	0.14	0	1.1	0.41	0.31	0
1D model Simulation	η (ms^{-1}.Oe^{-1})	0.11	0.11	0.11	0.125	0.14	?	0.097	0.13	0.15	0.18
	P^{**}	0.21	0.21	0.21	0.21	0.21	0.21	0.21	0.21	0.21	0.21
	u (m.s^{-1})	41	41	55	43	33	21	36	44	39	23
	Δ (nm)	4.5	4.3	4.6	4.8	5.2	6	4.4	4.9	5.3	6.7
	α^*	0.1	0.1	0.1	0.1	0.1	0.1	0.1	0.1	0.1	0.1
	β	0	0	0	0	0	0	0	0	0	0
	H_{DMI} (Oe)	1200	1400	1500	1750	1900	1500	900	1500	1700	1100
	H_{DW} (Oe)	1526	1641	1730	1525	1232	700	1694	1223	866	324
	δ_{DMI}	0.100	0.127	0.109	0.185	0.292	0.400	0.092	0.136	0.199	0.246
	D	5.178	5.055	4.899	4.414	4.107	2.481	4.777	3.766	2.883	1.228

3. Future plans

We are in the process of understanding the origin of J_c from our model of chiral spin torque and exchange coupling torque driven DW motion and in parallel continue to explore other materials to reduce J_c significantly. Materials with high spin Hall angles with e.g. materials with A15 structure such as β-W may be promising. Also the systems with skyrmion or skyrmion-like magnetic structures would bevgood candidates to move the DWs at very low threshold currents.

References

[1] Kwang-Su Ryu, Luc Thomas, See-Hun Yang, and Stuart Parkin, “Chiral Spin Torque at Magnetic Domain Walls”, Nat. Nano. 8, 527-533 (2013).

[2] Stuart Parkin and See-Hun Yang, “Memory on the Racetrack”, Nat. Nano. 10, 195-198 (2015).

[3] See-Hun Yang, Kwang-Su Ryu, and Stuart Parkin, “Domain-wall velocities of up to 750 m s−1 driven by exchange-coupling torque in synthetic antiferromagnets”, Nat. Nano. 10, 221-226 (2015).

[4] Malozemoff, A. & Slonczewski, J. “Magnetic domain walls in bubble materials” Academic Press, New-York, 1979.

[5] Hayashi, M., Thomas, L., Rettner, C., Moriya, R. & Parkin, S. S. P. “Direct observation of the coherent precession of magnetic domain walls propagating along permalloy nanowires”. Nat. Phys. 3, 21–26 (2007).

[6] Kwang-Su Ryu, See-Hun Yang, Luc Thomas, and Stuart Parkin, “Chiral spin torque arising from proximity induced magnetization”, Nat. Comm. 5, 3910 (2014).

[7] Tanaka, T, et al, “Intrinsic spin Hall effect and oribital Hall effect in 4d and 5d transition metals”, Phys. Rev. B 77, 165117 (2008).

[8] Yakata, S, Ando, Y, Miyazaki, T, and Mizukami, S., “Temperature dependecnes of spin-diffusion lengths of Cu and Ru layers, Jpn J. Appl. Phys. 45, (2006).

[9] Ryu, K.-S, Thomas, L., Yang, S.-H, & Parkin, S.S.P, “Current induced tilting of domain walls in high velocity motion along perpendicularly magnetized micron-sized Co/Ni/Co racetracks”, Appl. Phys, Exp. 5, 093006 (2012).

[10] O. Boulle, et al, “Domain wall Tilting in the Presence of the Dzyaloshinskii-Moriya Interaction in Out-of-Plane Magnetized Magnetic Nanotracks”, Phys. Rev. Lett. 111, 217203 (2013).

III. Role of domain wall tilting and chiral spin torque in current driven domain motion in Y-shaped nanowire racetracks

1. Introduction and Motivation

The controlled manipulation of domain walls (DWs) by current forms the basis of a number of proposed memory and logic devices, and a deep understanding of the dynamics of the DWs is crucial from both a scientific and technological standpoint[1,2]. In ultrathin magnetic heterostructures, the presence of spin-orbit coupling gives rise to chiral N*é*el walls magnetic media with perpendicularly magnetic anisotropy (PMA), which are stabilized by the Dzyaloshinskii-Moriya Interaction (DMI) [3,4,] and also to a highly efficient chiral spin torque mechanism[5,6]. In straight nanowires, the current-driven propagation of alternating *Néel* DWs without the presence of an in-plane field is equivalent, leading to the lock-step motion of several DWs in a nanowire. We have recently observed that by engineering the structure in which the DWs propagate, which in our case is in the shape of a Y-shaped junction[7], the DW propagation process becomes selective to the polarity of the DWs even in the absence of any externally applied magnetic fields.

2. Results and Discussion

Using polar Magneto-Optical Kerr Effect (MOKE) microscopy, we image (Fig. 1) the propagation of DWs under current from the input branch (labeled A) into two identical output branches (labeled B and C) and observe a large asymmetry in the DW propagation in the two output branches depending upon the polarity of the incoming DW. This asymmetry can be inverted by changing the configuration of the incoming DW. Moreover, we remarkably find that after splitting at the Y-shaped junction, the DW velocity in one branch remains largely unaffected compared to its initial velocity whereas simultaneously the DW velocity in the other branch can, in some cases, decrease by as much as 90%. We observe that this large change in the DW velocity in a particular branch depends on the relative angle between the local magnetization of the DW and the spin orbit torque (SOT) emanating from the underlying heavy-metal layer in these microwires. Surprisingly, we further find that the DW dynamics can take as much as 50-100ns to respond to the abrupt change in the SOT acting on it.

The devices shown in Fig. 8 have been patterned using standard lithography techniques from the magnetic stack: 10 AlOx | 2 TaN | 1.5 Pt | 0.3 Co | 0.7 Ni | 0.15 Co | 5 TaN | (the numbers indicate the respective film thickness in nm) grown by sputtering on Si substrates with a 25nm oxidized layer for electrical isolation. Care is taken so that there is minimal roughness along the edges of the structure so that both output branches B and C, with an angle θ between them, are nominally identical for DW motion. The input branch A is designed to be twice in width ($5\mu m$) as compared to the widths ($2.5\mu m$) of the two output branches B and C so as to keep the current density across the entire Y-shaped structure the same (the current crowding near the bifurcation point exists for less than 100 nm regions as obtained from finite element modeling). A nanosecond pulser is connected to the input branch whereas the two output branches are both grounded.

A DW is first created in branch A and is then moved towards the bifurcation point by a predetermined distance, d_A without any external magnetic field (see Fig. 8 first panel). Once the DW is in the correct location, the background MOKE contrast is reset. Afterwards, a single pulse of voltage V and pulse length t is applied

across the device, which makes the DW to move from its initial position in branch A, and to split into two DWs that then travel into the two output branches, represented by the Kerr contrast image. The distances traversed d_B and d_C by the two DWs in their respective two output branches B and C are then measured. This single-shot experiment for a given V and t is repeated 25-50 times to build statistics. The experiment is repeated for $10V \leq V \leq 28V$ and $20ns \leq t \leq 100ns$ for devices with $\theta = 30°, 60°, 90°$ and $120°$.

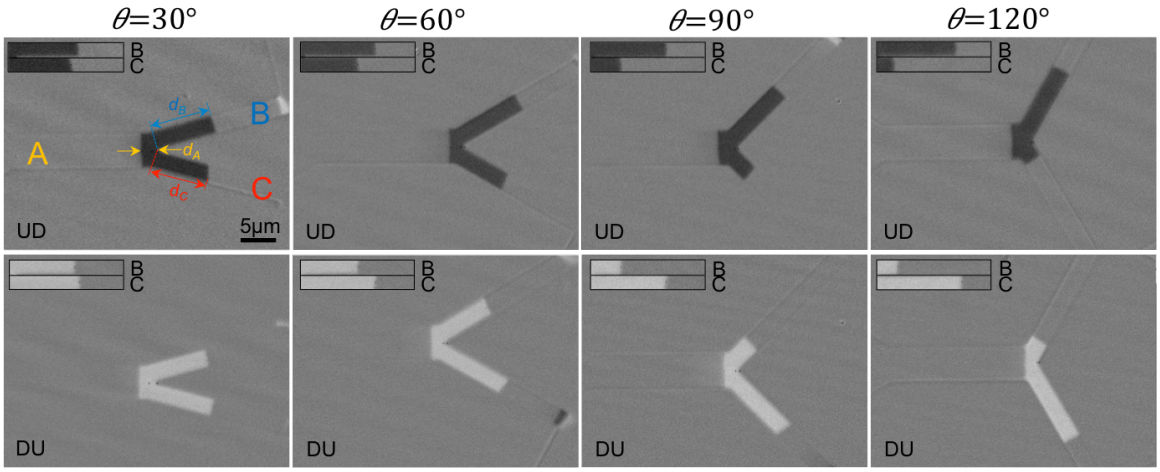

Figure 8. MOKE images of four different devices with increasing θ, which show the propagation of an UD DW (*top row*) and DU DW (*bottom row*) from branch A into branches B and C when an electrical pulse of 16V and 100ns is applied. The electrical pulser is connected to branch A, whereas both branches B and C are grounded for all the devices.

The two distances d_B and d_C differ from one another in a systematic way as a function of the V, t and θ, which is our main result. Figure 8 (*first row*) shows a representative MOKE image of an up-down (UD) DW that travels much further in branch B than in branch C as θ is increased after a $V = 16V$ and $t = 100ns$ pulse is applied across the magnetic structure. Most importantly, in the same device, a down-up (DU) DW travels further in the opposite branch C than in branch B as θ is increased for the same voltage pulse (Fig. 8 *second row*). Figure 9 show that for a given V, t and θ, $d_B(d_C)$ for the UD DW is the same as $d_C(d_B)$ for the DU DW. Consequently, the asymmetry of the distances traversed, $\Delta d_{BC} = d_B - d_C$, is of the same magnitude but of opposite sign for up-down and down-up DWs for a given pulse, which indicates that the asymmetry is not due to spurious effects such as lithographic patterning, edge pinning, current crowding near the bifurcation point, or any other inhomogeneity in the magnetic structure that would make one branch more favorable over the other for DW motion. We also independently measure DW velocities, u_V as a function of V after creating DWs in branches B and C for all the devices studied. The dashed lines (Fig. 9) obtained from these measurements indicate the distance that a DW would travel if it were moving at u_V. Clearly, we see that for a given V, the fast moving DW moves at the same velocity as u_V whereas, the slow moving DW when it enters the branch, moves much slower.

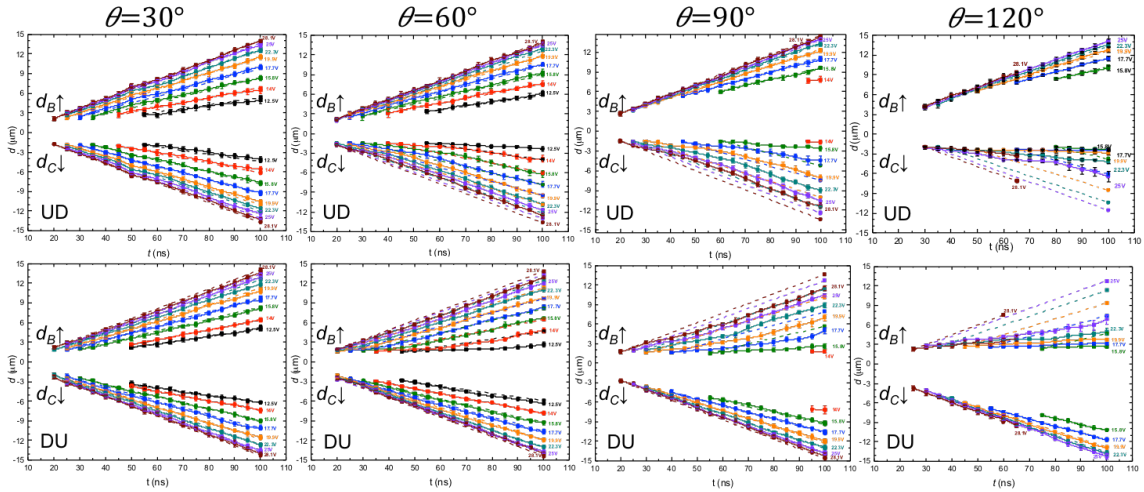

Figure 9. d_B and d_C deduced from the MOKE measurements (Fig. 1) for the four different devices with increasing θ, of an UD DW (*top row*) and DU DW (*bottom row*) for various V and t. The dashed lines represent the distances that a DW would travel if its velocity had not differed from u_V.

Furthermore, we note that for devices with $\theta = 30°, 60°, 90°$, Δd_{BC} increases for a certain amount of time, indicating that the DW velocity in one branch is higher than the other branch. Afterwards, Δd_{BC} becomes constant in time indicating that the DWs in the two branches move at the same velocity, namely, u_V. The time taken by the slow moving DW to accelerate to its normal velocity, u_V, decreases as V (current density; SOT) is increased, whereas it increases as θ is increased. Interestingly, for the device with $\theta = 120°$, no saturation in Δd_{BC} is observed even for the maximum V and t used in our experiments.

We exploit this newly discovered phenomenon to demonstrate domain sorting in one of the two output branches for a device with $\theta = 120°$ as shown in Fig. 10.

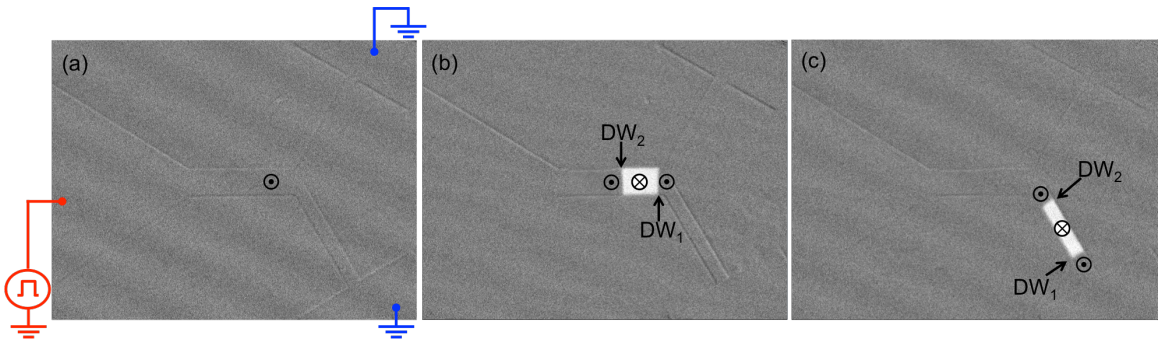

Figure 10. (a) Microwire PMA structure where the input branch is 5 μm wide, whereas the two output branches are each 2.5 μm wide. Each branch is 15 μm long. A nanosecond voltage pulser (red) is connected to the left input branch whereas the two identical output branches (in blue) that subtend an angle of 120 degrees between them are both grounded. **(b)** A down domain is first created in branch A, close to the bifurcation point and afterwards a single pulse of 25V and 100ns is applied across the device, which pushes the down domain only in the bottom output branch as shown in **(c)**.

3. Conclusion and Outlook

Next, we plan to develop a thorough understanding of the disparity of the DW velocity in the two branches due to the transient changes in SOT and DMI torques and their effect on DW momentum by micromagnetic simulations and by simultaneously also performing measurements on devices with varying widths and magnetic structures with bends rather than Y-junctions, for example. We also plan to study the disparity in the DW velocity in the recently discovered synthetic anti-ferromagnetic PMA structures[8], where we have shown that an entirely different exchange coupling torque is responsible for the DW dynamics.

References

1. Parkin, S. S. P., Hayashi, M. & Thomas, L. Magnetic Domain-Wall Racetrack Memory. *Science* **320,** 190–194 (2008).

2. Parkin, S. & Yang, S. H. Memory on the racetrack. *Nature Nanotechnology* **10,** 195–198 (2015).

3. Bode, M. *et al.* Chiral magnetic order at surfaces driven by inversion asymmetry. *Nature* **447,** 190–193 (2007).

4. Boulle, O. *et al.* Domain Wall Tilting in the Presence of the Dzyaloshinskii-Moriya Interaction in Out-of-Plane Magnetized Magnetic Nanotracks. *Phys. Rev. Lett.* **111,** 217203 (2013).

5. Emori, S., Bauer, U., Ahn, S.-M., Martinez, E. & Beach, G. S. D. Current-driven dynamics of chiral ferromagnetic domain walls. *Nat Mater* **12,** 611–616

6. Ryu, K.-S., Thomas, L., Yang, S.-H. & Parkin, S. Chiral spin torque at magnetic domain walls. *Nat Nano* **8,** 527–533 (2013).

7. Pushp, A. Domain wall trajectory determined by its fractional topological edge defects. *Nature Physics* **9,** 505–511 (2013).

8. Yang, S. H., Ryu, K. S. & Parkin, S. Domain-wall velocities of up to 750 ms− 1 driven by exchange-coupling torque in synthetic antiferromagnets. *Nature Nanotechnology* **10,** 221–226 (2015).